A&A manuscript no.
(will be inserted by hand later)

Your thesaurus codes are:
03(11.01.2; 11.02.1; 13.18.1; 13.25.2)

ASTRONOMY
AND
ASTROPHYSICS
30.11.1995

ROSAT Observations of BL Lacertae Objects

G. Lamer[1], **H. Brunner**[1,2], **and R. Staubert**[1]

[1] Institut für Astronomie und Astrophysik, Abt. Astronomie, Universität Tübingen, Waldhäuserstr. 64, D-72076 Tübingen, Germany
[2] Astrophysikalisches Institut Potsdam, An der Sternwarte 16, D-14482 Potsdam, Germany

Received ; accepted

Abstract. We present soft X-ray spectra of 74 BL Lacertae objects observed with the PSPC detector on board of the ROSAT satellite. The sample contains all BL Lac objects detected during the pointed observation phase as a target or serendipitously. We have investigated the soft X-ray and broad band spectral properties and discuss the consequences for the X-ray emission processes. For the first time a clear dependence of the X-ray spectral steepness on the radio to X-ray spectral energy distribution is found: $\alpha_{\rm rx}$ and $\alpha_{\rm x}$ are *correlated* in the X-ray selected (XBL) subsample and *anticorrelated* in the radio selected (RBL) subsample. The objects with intermediate $\alpha_{\rm rx}$ values thus do have the steepest soft X-ray spectra. Simulated PSPC spectra based on a set of simple two component multifrequency spectra are in good agreement with the measurements and suggest a broad range of synchrotron cutoff energies.

We have calculated synchrotron self-Compton beaming factors for a subsample of radio bright objects and find a correlation of the beaming factors $\delta_{\rm IC}$ with $\alpha_{\rm rx}$ and $\alpha_{\rm x}$. The most extreme RBL objects are very similar to flat spectrum radio quasars in all their broad band and X-ray properties.

Key words: Galaxies: active – BL Lacertae objects: general – Radio continuuum: galaxies – X-rays: general

1. Introduction

BL Lac objects are active galactic nuclei which by definition do not have strong emission lines, are highly variable, and show strong polarization in the radio to optical emission. Commonly the properties of BL Lacs are explained by the concept that the emission in all spectral bands is dominated by relativistic jets. Relativistic electrons emit synchrotron radiation and may scatter up either synchrotron photons (synchrotron self-Compton emission) or photons from other regions (e.g. from an accretion disc) to higher energies.

Originally most BL Lacs have been found as counterparts of flat spectrum radio sources (radio selected BL Lacs, RBLs), but an increasing number of less radio bright objects were discovered by the identification of X-ray sources (XBLs). Due to the lack of spectral features in the optical no complete optically selected samples exist. The total number of BL Lac objects in the catalogue of Véron-Cetty & Véron (1993) is less than 200. A new catalogue consisting of 233 sources is being published by Padovani & Giommi (1996a). The ongoing search for new BL Lacs from ROSAT sources (Kock et al. 1996, Nass et al. 1996) will significantly increase the number of known objects.

Recently BL Lacs have gained great interest due to the detection of several objects in high energy γ-rays by EGRET on the Compton Gamma Ray Observatory (von Montigny et al. 1995).

There is some evidence that RBLs and XBLs form distinct subclasses as they show a bimodal distribution in the plane of the broad band spectral indices $\alpha_{\rm ro}$ versus $\alpha_{\rm ox}$ (e.g. Giommi et al. 1990). Regardless of the discovery waveband we will use these terms for a distinction of the subclasses based on the spectral energy distribution: RBL is used for *radio* bright objects having $\alpha_{\rm rx}>0.75$ and XBL for *X-ray* bright objects with $\alpha_{\rm rx}<0.75$.

There have been several attempts to explain the physical differences of the XBL and RBL objects and their relation to flat spectrum radio quasars (FSRQs). The concept that parts of the continuum emission from radio loud AGN arises from jets of radiogalaxies more or less aligned with the line of sight is widely accepted.

Based on the study of number count relations and luminosity functions several authors (e.g. Padovani & Urry 1990) proposed that BL Lacs are the beamed subpopulation of FR I galaxies with RBLs having higher beaming factors than XBLs. Ghisellini & Maraschi (1989) discussed an "accelerating jet" model with lower bulk Lorentz factors Γ in the X-ray emitting regions resulting in broader beaming cones for the X-ray emission and narrow radio cones. Celotti et al. (1993) developed a "wide jet" model with geometrically wider opening angles in the inner, X-ray emitting, parts of the jet. Assuming that RBLs have smaller viewing angles than XBLs, both models are able to explain both the relative numbers and different spectral energy distributions of XBLs and RBLs with an intrinsically uniform population of objects. Maraschi & Rovetti (1994) have extended these considerations on FSRQs and propose that all radio loud AGN

Send offprint requests to: G. Lamer

only essentially differ in viewing angle and intrinsic power of the central engine.

An alternative approach to explain the differences between XBLs and RBLs was made by Padovani & Giommi (1995) with a “different energy cutoff” hypothesis. They argue that both types form a uniform class of objects spanning a wide range in the intrinsic energy distribution caused by different cutoff frequencies of the synchrotron component.

The X-ray spectra of RBLs in average were found to be significantly steeper than the spectra of (higher redshifted) FSRQs in *Einstein* IPC (Worrall & Wilkes 1990) and ROSAT PSPC (Brunner et al. 1994) investigations. Furthermore, the X-ray spectral indices of BL Lacs showed a broad distribution in both investigations. The mean X-ray spectra of XBLs and RBLs were not found to be significantly different in *Einstein* IPC (Worrall & Wilkes 1990), EXOSAT ME + LE (Sambruna et al. 1994), and ROSAT PSPC (Lamer et al. 1994) observations. Ciliegi et al. (1995) found significant steepening of the mean spectrum of XBLs between the soft (0.2–4 keV) and medium (2–10 keV) energy X-ray band.

The ROSAT data archive presently comprises the largest X-ray database for BL Lac objects collected by a single instrument. In this paper we present the analysis of X-ray and broad band spectra of 74 BL Lac objects with the X-ray data obtained from pointed ROSAT observations. We find a strong interdependence of the X-ray spectral index α_x with the radio to X-ray energy index α_{rx} which we interprete as the signature of two spectral components intersecting each other at different frequencies.

2. The sample

Due to the difficulties in the identification and classification of BL Lacs only relatively few objects form complete flux limited samples. Nearly complete samples were selected from radio sources (1 Jy sample, Stickel et al. 1991; 34 objects) and with limited sky coverage from soft X-ray sources (EMSS sample, Morris et al. 1991; 22 objects). Our sample comprises all BL Lacs listed in the catalogue of Véron-Cetty & Véron (1993) and of which ROSAT PSPC observations exist in the archives. Only sources which had been detected with more than 50 net counts have been analysed: 74 objects in total. In case of multiple ROSAT observations of an object the longest observation available at the time of analysis has been selected. Objects in the catalogue which have meanwhile been classified as quasars or as radio galaxies have not been included (e.g. Stickel et al. 1994). The resulting coverage of various complete samples of BL Lac objects is listed in Table 1. According to their radio to X-ray energy distribution 40 objects have been assigned to the XBL subsample, 34 objects to the RBL subsample (see Sect. 3).

Throughout this paper the catalogue designations according to Véron-Cetty & Véron (1993) are used.

Table 1. Coverage of complete samples

sample	Reference	observed (total)
1 Jy (5 GHz)	Stickel et al. (1991)	29 (34)
EMSS	Morris et al. (1991)	19 (22)
S5 ($\delta > 70°$)	Eckart et al. (1986)	5 (5)

3. ROSAT observations and data analysis

Archival data were taken from the ROSAT data archives at MPE (Garching) and at GSFC (Greenbelt). Both the author’s proprietary data and archival data were reduced in the same way using the EXSAS software (Zimmermann et al. 1993). Table 2 list the objects, ROSAT observation request (ROR) numbers, and dates of observations which have been analysed.

The source photons were extracted within a circle of radius 100”–200” (depending on the signal to noise ratio) and the background determined in an annulus of radii 250” and 500”. We produced spectra in the energy range 0.1–2.4 keV of all objects by binning according to pulse height amplitude, yielding a SNR per spectral bin ranging from 4 for the weakest sources and 50 for the strongest. All spectra were background subtracted and corrected for telescope vignetting, dead time losses, and incomplete extraction of source photons with respect to the point spread function. The pulse height spectra were then fitted by power law spectra combined with the absorption model of Morrison and McCammon (1983). For sources with more than 250 detected counts both fits with an absorbing column density N_H fixed to the galactic value (Stark et al. 1992, Elvis et al. 1989) and free N_H were performed. For the weaker sources only fits with fixed N_H were obtained.

In general the latest version of the PSPC detector response matrix (nr. 36) has been used for the fits. Except for observations carried out before fall 1991, when the gain setting of the PSPC was different, an earlier version (nr. 6) was used.

We combined the ROSAT measurements with noncontemperaneous flux measurements at 5 GHz and in the optical V band (both taken from Véron-Cetty & Véron) in order to calculate the broad band spectral indices α_{rx} , α_{ro} , and α_{ox} . Sources with $\alpha_{rx} > 0.75$ were assigned to the RBL subsample and sources with $\alpha_{rx} < 0.75$ to the XBL subsample.

Power law spectral indices α are given as energy indices ($f_\nu \propto \nu^{-\alpha}$) throughout the paper.

We used a maximum likelihood (ML) method to deconvolve the measurement errors and the intrinsic distribution of the X-ray spectral indices and other measured parameters when calculating mean values and their errors (see Worrall 1989 for a description of the method and Brunner et al. 1994 as a recent application). Assuming that both the intrinsic distribution of a parameter p and the distribution of measurement errors are Gaussian, confidence contours of the mean $\langle p \rangle$ and width σ_G of the intrinsic distribution of p can be calculated.

Table 2. List of PSPC observations

Object	ROR number	completed date	expos. [sec]	net counts
PKS 0048-09	701433	04-jul-93	8363	3368 ± 59
PKS 0118-27	701427	10-jul-93	2635	366 ± 21
MS 0122+09	700976	16-jul-92	11173	208 ± 21
MS 0158+00	700972	24-jul-92	1646	1113 ± 35
MS 0205+35	700977	12-aug-92	13964	2644 ± 54
3C 66A	600019	18-aug-91	24880	5182 ± 125
AO 0235+16	701379			
	– ...385	06-aug-93	14591	2694 ± 53
MS 0257+34	700309	27-jan-92	7434	229 ± 21
PKS 0301-24	701503	10-aug-93	3412	936 ± 32
MS 0317+18	700971	24-aug-92	2917	412 ± 22
H 0323+02	700099	24-aug-91	25727	13156 ± 129
MS 0331-36	700921	05-feb-93	6214	424 ± 24
1ES 0347-12	900492	28-jul-93	9620	7817 ± 92
MS 0350-37	701508	13-aug-93	5589	1227 ± 39
PKS 0406+12	700825	24-feb-93	15749	214 ± 16
1H 0413+00	701055	31-aug-92	9043	10315 ± 103
MS 0419+19	700044	26-feb-91	4704	656 ± 28
PKS 0426-38	701428	02-aug-93	4048	211 ± 18
S5 0454+84	701058	17-aug-93	14850	63 ± 10
PKS 0537-44	700199	10-apr-91	2598	918 ± 31
PKS 0548-32	700487	06-mar-92	9600	35371 ± 189
MS 0607+71	700111	13-mar-91	14086	247 ± 27
S5 0716+71	700210	08-mar-91	21043	16236 ± 128
PKS 0735+17	700829	28-oct-92	6684	592 ± 30
MS 0737+74	800230	12-mar-93	8782	4455 ± 71
PKS 0820+22	700831	29-oct-92	3728	64 ± 9
OJ 448	700832	04-oct-92	4821	59 ± 11
OJ 287	700219	16-apr-91	3622	998 ± 33
B2 0912+29	700224	24-apr-91	2897	1172 ± 35
MS 0922+74	700311	25-mar-92	4137	463 ± 24
S4 0954+65	700042	17-apr-91	6772	343 ± 21
GB 1011+49	700220	11-may-91	5234	10204 ± 104
1ES 1028+51	701544	22-oct-93	10783	23508 ± 157
MARK 421	700513	05-may-92	35838	$5.698 \cdot 10^6$
MARK 180	700427	18-nov-91	3096	6117 ± 80
PKS 1144-37	701434	07-jul-93	7747	852 ± 32
B2 1147+24	701181	01-dec-92	4370	2842 ± 55
1207+39W4	700277	31-may-91	38127	7180 ± 87
B2 1215+30	700221	15-jun-91	21999	10141 ± 107
GB2 1217+34	700222	22-may-93	4281	282 ± 23
1H 1219+301	701056	18-jun-92	10969	52488 ± 230
ON 231	700223	14-jun-91	15223	3318 ± 64
MS 1221+24	700308	19-dec-91	5624	845 ± 33
MS 1229+64	700974	03-dec-92	3034	2499 ± 51
B2 1308+32	700216	23-jun-92	8386	784 ± 34
MS 1332-29	600188	28-jan-92	2007	207 ± 15
MS 1402+04	700310	17-jan-92	4763	2876 ± 59
MS 1407+59	200406	10-may-91	4645	491 ± 28
1E 1415+25	150071	16-jul-90	18861	22242 ± 157
OQ 530	150046	19-jul-90	11516	2485 ± 55
PKS 1424+24	701504	11-jul-93	3065	1791 ± 44
H 1426+42	700535	24-jan-92	9593	37670 ± 197
MS 1443+63	700975	18-jul-92	4208	663 ± 29
MS 1458+22	700312	19-jan-92	4557	1694 ± 44
PKS 1519-27	701430	17-aug-93	2552	262 ± 17
4C 14.60	700834	28-jan-93	7215	282 ± 21
MS 1552+20	700973	26-aug-92	3562	2971 ± 56
MARK 501	700130	25-feb-91	7649	51150 ± 227
MS 1704+60	700439	28-oct-91	13068	1090 ± 49
I ZW 187	701151	02-oct-92	4548	7015 ± 85
S4 1749+70	700835	09-nov-92	3702	316 ± 21
OT 081	700043	28-mar-92	9507	747 ± 31
S5 1803+78	700497	07-apr-92	6911	539 ± 24
3C 371.0	700489	09-apr-92	10461	1182 ± 35
4C 56.27	700837	19-jun-92	5900	818 ± 31
PKS 2005-48	700488	27-apr-92	11487	33094 ± 177
PKS 2005-48	701057	28-oct-92	11462	18747 ± 138
S5 2007+77	700498	11-dec-91	9525	443 ± 22
PKS 2131-02	701431	02-nov-93	7748	130 ± 15
MH 2136-42	701180	26-apr-93	3798	576 ± 25
MS 2143+07	700045	09-may-91	3526	748 ± 31
PKS 2155-30	700507	12-nov-91	52643	$2.396 \cdot 10^6$
BL LAC	700838	22-dec-92	2167	356 ± 19
PKS 2240-26	701432	09-nov-93	3656	178 ± 16

4. Results of spectral analysis

The distribution of α_{rx} (Fig. 1) is double peaked with a gap at $\alpha_{rx} = 0.6$–0.8. As can been seen from Fig. 1, all EMSS objects exhibit an XBL energy distribution. Two objects of the 1 Jy sample have $\alpha_{rx} < 0.75$, they therefore belong to the XBL sample. This confirms, based on homogeneus X-ray data, the relations given by Padovani & Giommi (1995).

Figure 7 shows the interdependence of the calculated broad band spectral indices α_{ox} and α_{ro}. Note that the gap near $\alpha_{rx} = 0.75$ is dominated by objects which do neither belong to the EMSS sample nor to the 1 Jy sample. This indicates that the gap is due to selection effects and may be filled in the future when radio or X-ray selected objects at lower flux limits will be identified.

Single power law spectra with photoelectric absorption due to the interstellar medium in general yielded acceptable fits if the absorbing column density N_H was left free to vary. The results of the spectral fits with free N_H and the broad band spectral indices are given in Table 3. If a source was detected with less than 250 counts, the entry $N_{H,fit}$ is omitted and the results with fixed N_H are given. In order to investigate whether deviations of the resulting N_H values from galactic HI radio measurements are significant we calculated the difference ΔN_H for each object. The error of the difference was calculated by quadratic addition of the X-ray and radio measurement errors using $10^{20}\mathrm{cm}^{-2}$ for the Stark et al. (1992) values and $10^{19}\mathrm{cm}^{-2}$ for the Elvis et al. (1989) values. A maximum likelihood analysis of the results yields a mean N_H-excess of $(0.48 \pm 0.23) \cdot 10^{20}\mathrm{cm}^{-2}$ in the XBL sample. In the RBL sample the individual errors of the

Table 3. X-ray and broad band spectra

Object	$N_{\rm H,gal}$	$N_{\rm H,fit} \pm 1\sigma$	$F_{\rm 1keV}$	$\alpha_{.1-2.4\rm keV}$	$\alpha_{\rm rx}$	$\delta_{\rm IC}$
	$[10^{20}{\rm cm}^{-2}]$		$[\mu$Jy$]$	$\pm 1\sigma$		
PKS 0048-09	4.92	4.13±0.53	0.91	1.70±0.16	0.82	
PKS 0118-27	1.60	2.80±1.59	0.19	1.84±0.45	0.86	
MS 0122+09	4.33		0.06	0.47±0.40	0.55	
MS 0158+00	2.54	2.60±0.74	1.32	1.33±0.23	0.51	
MS 0205+35	6.27	13.95±0.97	0.28	1.50±0.32	0.54	
3C 66A	8.89	12.27±0.84	0.93	1.46±0.32	0.79	0.07
AO 0235+16	8.64	23.08±1.77	0.65	1.46±0.49	0.86	5.13
MS 0257+34	10.30		0.13	1.70±0.39	0.64	
PKS 0301-24	2.27	1.43±0.61	0.27	1.68±0.31	0.80	
MS 0317+18	10.16	8.80±2.45	0.57	1.31±0.67	0.58	
H 0323-02	8.68[a]	8.30±0.60	3.21	1.27±0.09	0.57	
MS 0331-36	1.39	2.15±1.30	0.34	1.20±0.49	0.58	
1ES 0347-12	3.69	3.58±0.33	2.56	1.12±0.09	0.45	
MS 0350-37	1.45	1.52±0.61	0.35	1.17±0.26	0.61	
PKS 0406+12	14.83		0.05	0.79±0.45	0.97	
1H 0413+00	9.15[a]	9.18±0.50	4.64	1.55±0.10	0.55	
MS 0419+19	17.50	20.13±22.3	0.77	0.58±0.87	0.52	
PKS 0426-38	1.92		0.09	2.28±0.18	0.93	
S5 0454+84	5.60		0.02	0.87±0.59	1.01	3.40
PKS 0537-44	4.37	2.94±0.09	0.81	1.18±0.25	0.87	8.97
PKS 0548-32	2.49[a]	2.76±0.14	9.59	0.95±0.05	0.57	
MS 0607+71	9.63		0.08	1.45±0.48	0.70	
S5 0716+71	3.73	3.00±0.20	1.26	1.75±0.06	0.77	1.20
PKS 0735+17	4.35[a]	2.70±1.32	0.24	0.77±0.39	0.90	7.70
MS 0737+74	3.29	4.16±0.48	1.61	1.39±0.11	0.54	
PKS 0820+22	3.92		0.05	1.05±0.47	0.98	
OJ 448	3.89		0.04	0.68±0.63	0.97	
OJ 287	2.75[a]	2.52±0.80	0.62	1.09±0.29	0.86	10.56
B2 0912+29	2.82	1.57±0.55	0.58	1.31±0.24	0.72	
MS 0922+74	1.91	2.81±1.34	0.27	1.03±0.45	0.53	
1E 0950+49	1.06	1.11±0.53	0.30	1.45±0.27	0.52	
S4 0954+65	4.30	12.30±3.42	0.23	1.06±1.09	0.89	5.86
GB 1011+49	0.80	1.35±0.17	2.15	1.49±0.08	0.67	
1E 1028+51	1.09	1.33±0.13	2.55	1.44±0.05	0.56	
MARK 421	1.61[a]	2.03±0.01	272.8	1.37±0.01	0.44	0.29
MARK 180	1.27[a]	1.87±0.26	2.62	1.51±0.10	0.66	
PKS 1144-37	8.74	10.33±2.87	0.46	1.74±0.46	0.87	

Table 3. – Continued

Object	$N_{\rm H,gal}$	$N_{\rm H,fit} \pm 1\sigma$	$F_{\rm 1keV}$	$\alpha_{.1-2.4\rm keV}$	$\alpha_{\rm rx}$	$\delta_{\rm IC}$
	$[10^{20}{\rm cm}^{-2}]$		$[\mu$Jy$]$	$\pm 1\sigma$		
B2 1147+245	1.90	2.52±0.46	1.33	1.25±0.15	0.76	0.20
1207+39W4	1.82	3.51±0.34	0.51	1.15±0.09	0.53	
B2 1215+303	1.60[a]	2.16±0.23	0.49	1.88±0.08	0.77	0.30
GB2 1217+34	1.14	0.94±1.54	0.10	0.98±0.71	0.81	
1H 1219+301	1.78[a]	2.51±0.10	10.05	1.22±0.03	0.48	
ON 231	1.88	2.13±0.41	0.40	1.24±0.16	0.81	0.24
MS 1221+24	4.45	1.76±0.80	0.20	1.51±0.34	0.67	
MS 1229+64	1.96	3.16±0.56	2.21	1.02±0.16	0.56	
B2 1308+32	1.10[a]	1.31±0.77	0.15	1.02±0.34	0.91	7.72
MS 1332-29	3.98		0.34	1.14±0.21	0.59	
MS 1402+04	2.07	2.84±0.53	0.71	2.03±0.15	0.57	
MS 1407+59	1.36	2.50±1.56	0.11	2.07±0.49	0.67	
1E 1415+25	2.29	2.15±0.15	3.34	1.19±0.06	0.55	
OQ 530	1.52	1.26±0.37	0.32	1.09±0.17	0.85	
PKS 1424+24	1.65	5.34±0.81	1.26	2.18±0.16	0.70	
H 1426+42	2.03	1.46±0.09	6.86	1.05±0.04	0.49	
MS 1443+63	1.57	3.02±1.11	0.39	1.09±0.36	0.58	
MS 1458+22	3.45	5.80±0.09	0.81	2.26±0.16	0.59	
PKS 1519-27	8.72	10.50±3.06	0.44	1.28±0.99	0.87	18.69
4C 14.60	3.35	4.02±2.17	0.12	0.90±0.72	0.94	1.37
MS 1552+20	4.06[a]	3.95±0.57	2.62	0.74±0.15	0.54	
MARK 501	1.73	2.87±0.11	24.73	1.77±0.03	0.62	1.29
1E 1704+60	2.40	2.50±1.10	0.16	1.36±0.35	0.53	
I ZW 187	2.58[a]	3.43±0.34	3.63	1.39±0.08	0.61	0.01
S4 1749+70	3.72	2.01±1.54	0.16	1.23±0.60	0.89	
B OT 081	9.20	6.94±4.40	0.30	0.47±0.30	0.88	14.78
S5 1803+78	4.30	5.16±1.35	0.23	1.16±0.34	0.92	7.92
3C 371	4.67	3.43±0.81	0.32	0.87±0.25	0.88	0.81
4C 56.27	3.85	6.46±0.71	0.52	0.60±0.34	0.85	
S5 2007+77	8.80	9.50±4.00	0.20	0.86±0.77	0.89	4.24
PKS 2005-48	5.44	3.84±0.14	4.00	1.91±0.03	0.71	
PKS 2131-02	3.92		0.05	0.85±0.37	0.99	
MH 2136-42	2.94	2.23±1.15	0.12	2.20±0.41	0.77	
MS 2143+07	4.98	7.52±1.82	0.77	1.52±0.39	0.63	
PKS 2155-30	1.35[a]	1.41±0.04	46.00	1.63±0.02	0.50	
BL LAC	20.15	33.84±3.37	1.46	2.01±1.60	0.82	4.00
PKS 2240-26	1.54		0.07	1.24±0.20	0.93	

[a] Elvis et al. 1989, other values: Stark et al. 1992

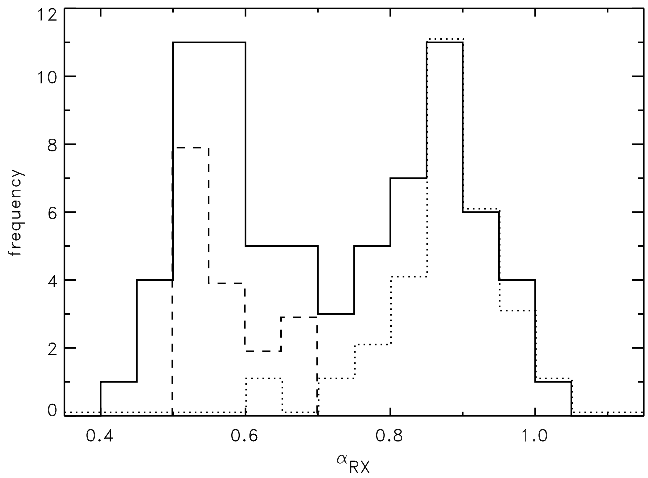

Fig. 1. Distribution of α_{rx} in the full sample (solid line), in the EMSS sample (dashed), and in the 1Jy sample (dotted line).

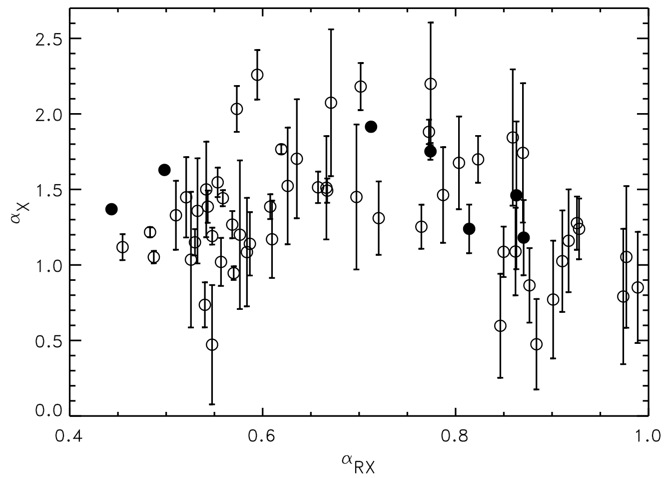

Fig. 2. X-ray spectral index α_x versus broad band index α_{rx} , sources with errors $\Delta\alpha_x < 0.5$ only, filled circles: EGRET detected objects

fitted N_H values are generally large and therefore no statement about deviations from galactic N_H can be made. Note that due to poor energy resolution in the soft band of the PSPC an apparent excess of N_H may also be caused by a steepening of the intrinsic spectrum.

As for the fainter objects the statistical error of the measured α_x is of the same order as the expected variations within the sample, we used the maximum likelihood method to deconvolve the measurement errors and the intrinsic distribution of the X-ray spectral indices.

We find $\langle\alpha\rangle = 1.30 \pm 0.13$, $\sigma_G = 0.32 \pm 0.12$ for the RBL sample (34 objects) and $\langle\alpha\rangle = 1.40 \pm 0.09$, $\sigma_G = 0.32 \pm 0.07$ for the XBL sample (40 objects).

Although no significant difference can be found between the mean spectra of RBLs and XBLs, there is a dependence of the spectral index on the characterising parameter α_{rx} . As can be read from Fig. 2, objects with extreme values of α_{rx} on both sides tend to have flatter X-ray spectra than intermediate objects. For the RBLs ($\alpha_{rx} > 0.75$) a Spearman Rank test yields an *anti*correlation of α_x and α_{rx} with 99.9% probability. For the XBLs ($\alpha_{rx} < 0.75$) the significance of the positive correlation is 98%. The steepest X-ray spectra are therefore found for objects which fall into the gap between XBLs and RBLs ($0.6 < \alpha_{rx} < 0.8$) for which X-ray spectral indices up to $\alpha_x \sim 2.0$ are measured.

In a previous paper (Brunner et al. 1994) we stated that the mean X-ray spectral index $\langle\alpha_x\rangle$ of RBLs is similar to the mean optical to X-ray spectral slope $\langle\alpha_{ox}\rangle$, whereas the mean X-ray spectrum of FSRQs is significantly flatter than their optical to X-ray broad band spectrum. However, a relatively large dispersion of the differences $\alpha_{ox} - \alpha_x$ was found within the RBL sample. In the larger sample presented here a dependence of $\alpha_{ox} - \alpha_x$ on α_{rx} is visible (Fig. 6). XBLs show a steepening of the spectrum ($\alpha_{ox} - \alpha_x < 0$), whereas RBLs can exhibit both steepening or flattening, depending on α_{rx} . This explains the mean $\langle\alpha_{ox} - \alpha_x\rangle$ being zero with a large dispersion of the individual values in an RBL sample. The extreme RBLs ($\alpha_{rx} \sim 0.9$) exhibit spectral flattening of the same amount as FSRQs ($\alpha_{ox} - \alpha_x = 0.6$, Brunner et al. 1994).

The spectral results are available as a more detailed version of Tab. 3 via WWW (http://astro.uni-tuebingen.de/prepre/), where also an electronic version of this paper can be found.

5. Simulated spectra

The dependence of the X-ray spectral index on the radio to X-ray broad band index α_{rx} can be explained qualitatively by a two component spectrum as resulting from synchrotron self-Compton jet models (e.g. Königl 1981, Ghisellini et al. 1985). The correlated variations in α_{rx} and α_x are then caused by a varying high frequency cutoff of the synchrotron component.

In order to test this hypothesis we simulated ROSAT PSPC spectra with a simple two component spectrum as a sum of a parabolically steepening soft component C_S and power law hard component C_H (see Fig. 3):

$$C_S(\nu) = 1 \qquad \text{for } \nu < \nu_1$$

$$\log_{10} C_S(\nu) = \left(\frac{\log_{10}\nu_1 - \log_{10}\nu}{\log_{10} a}\right)^{\eta} \qquad \text{for } \nu > \nu_1$$

$$C_H(\nu) = N \cdot \nu^{\alpha_H}$$

Below ν_1 the soft component C_S mimics the flat radio spectrum which BL Lacs have in common; above ν_1 C_S is a parabola in the $\log \nu - \log f_\nu$ plane. The normalization N of the hard component was chosen so that C_H (1keV) and C_S (5 GHz) result in a given $\alpha_{rx,max}$. The extent of the soft component can be varied with the parameter a. Figure 3 shows the set of calculated spectra using the parameters from Tab. 4.

From the resulting spectra corresponding ROSAT PSPC pulse height spectra were determined by applying a galactic absorption model (Morrison & McCammon 1983) with $N_H = 3 \cdot 10^{20} \mathrm{cm}^{-2}$ and folding the spectra with the PSPC efficiency and detector response matrix. The resulting pulse height spectra

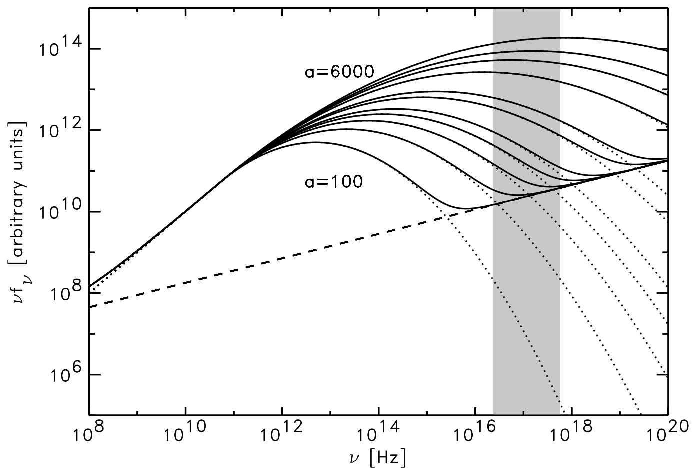

Fig. 3. Model spectra used for the simulations. Dotted: C_S , dashed: C_H , solid: total, shaded area: ROSAT PSPC energy range

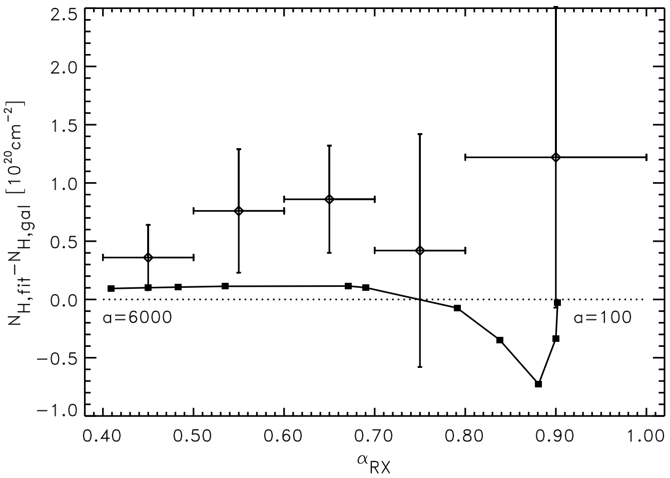

Fig. 5. Comparison of simulated (filled squares and solid line) and measured (diamonds with error bars) spectra in the α_{rx} – ΔN_H plane. The measured ΔN_H values were averaged in the bins indicated by the horizontal bars

Table 4. Parameters of model spectra

ν_1	η	α_H	$\alpha_{rx,max}$		
$5 \cdot 10^{10}$	2.00	0.70	0.90		
Sequence of variable parameter a:					
100	200	300	400	500	800
1000	2000	3000	4000	6000	

were fitted with an absorbed power law model in the same way as the BL Lac spectra. Broad band spectral indices α_{rx} , α_{ro} , and α_{ox} were determined from the flux values at 5 GHz, 5517Å, and 1 keV of each spectrum.

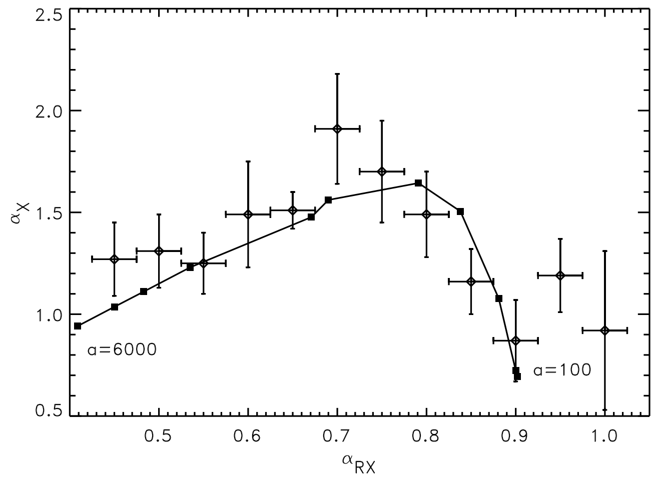

Fig. 4. Comparison of simulated (filled squares and solid line) and measured (diamonds with error bars) spectra in the $\alpha_{rx} - \alpha_x$ plane. The measured spectra were averaged in bins of $\Delta\alpha_{rx}$ =0.05.

The locations of simulated and observed spectra in the α_{rx} – α_x plane are plotted in Fig. 4. Mean values of α_x with 1σ errors have been determined in each α_{rx} interval using maximum likelihood contours. We find that the two component model is able to reproduce the measured interdependence of α_{rx} and α_x . As curvature of the incident photon spectra is able to cause deviations of the N_H values resulting from single power law fits, we also compared the resulting N_H in the simulated and measured spectra. The deviations in N_H as derived from the simulations are small ($< 6 \cdot 10^{19}\mathrm{cm}^{-2}$) and thus are hard to detect in individual spectra. Averaging the ($N_H - N_{H,gal}$) values in bins of α_{rx} using the ML method results in an overall excess of the measured N_H values (Fig. 5) over the simulations. Possibly this excess is caused by intrinsic absorption in individual sources.

The simulations are able to reproduce the measured dependence of the change in the spectral slope between the optical to X-ray broad band spectrum and the X-ray spectrum, ($\alpha_{ox} - \alpha_x$) on α_{rx} (Fig. 6).

Note that the α_{rx} values of the simulated spectra cannot exceed $\alpha_{rx,max}$, which was set to 0.9. Therefore with this parameter set the model does not cover objects with higher α_{rx} (Figs. 2 – 6). However, the number of objects with α_{rx} significantly exceeding 0.9 is small (Fig. 2).

In order to test whether the two component models do fit the whole radio to X-ray continuum, the broad band spectral indices α_{ox} and α_{ro} of simulated and object spectra were compared (Fig. 7). The path of the model spectra with varying parameter a in the α_{ox} – α_{ro} plane reasonably well reproduces the distribution of the measured broad band spectra.

6. Inverse Compton beaming factors

As inverse Compton beaming factors δ_{IC} are often used to estimate the viewing angles of radio sources, we investigated the dependency of δ_{IC} on α_{rx} and α_x in our sample.

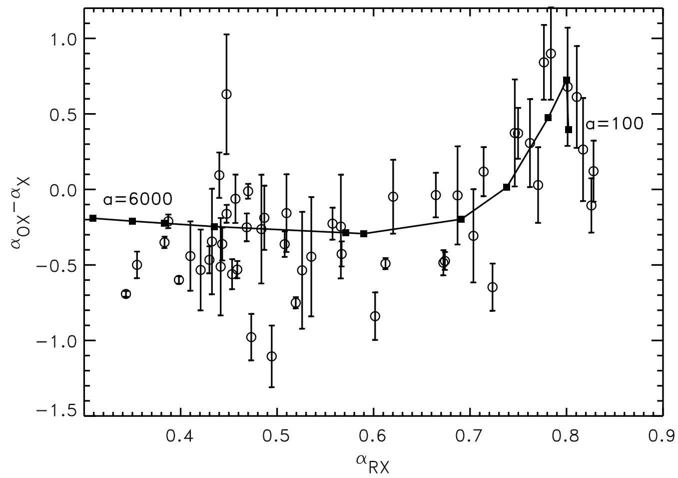

Fig. 6. Flattening ($\alpha_{\rm ox} - \alpha_{\rm x} > 0$) or steepening ($\alpha_{\rm ox} - \alpha_{\rm x} < 0$) of the X-ray spectra with respect to optical to X-ray broad band spectra vs. $\alpha_{\rm rx}$. Circles: measured spectra with errors $\Delta(\alpha_{\rm ox} - \alpha_{\rm x}) < 0.4$), filled squares and solid line: simulated spectra.

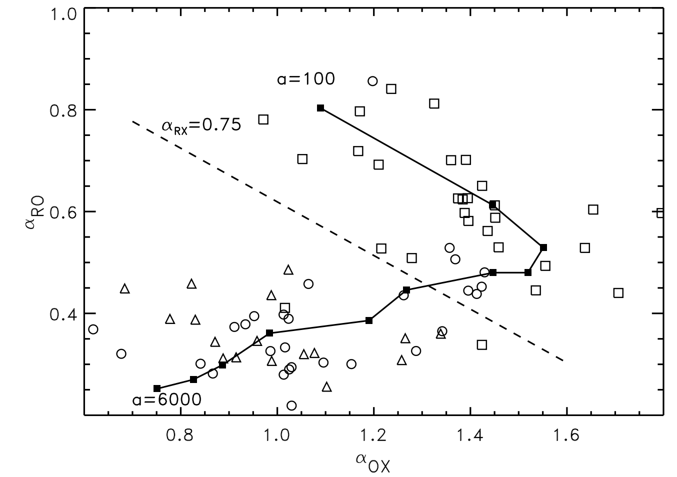

Fig. 7. Locations of object and simulated broad band spectra in the $\alpha_{\rm ox} - \alpha_{\rm ro}$ plane. Triangles: EMSS sample, rectangles: 1 Jy sample, circles: others, filled squares and solid line: simulated spectra. The division between XBLs and RBLs ($\alpha_{\rm rx}$ =0.75) is marked by the dashed line.

The Doppler beaming factor δ in a relativistic jet can be estimated by the condition that the inverse Compton flux from synchrotron self-Compton models must not exceed the observed X-ray flux. A method for the calculation of $\delta_{\rm IC}$ from radio brightness temperature and X-ray flux was given by Marscher (1987):

$$\delta_{\rm IC} = f(\alpha) F_{\rm m} \left(\frac{\ln(\nu_{\rm b}/\nu_{\rm m})}{F_{\rm x}\theta_{\rm d}^{6+4\alpha}\nu_{\rm x}^{\alpha}\nu_{\rm m}^{5+3\alpha}} \right)^{1/(4+2\alpha)} \cdot (1+z) \qquad (1)$$

$F_{\rm m}$ [Jy]: Synchrotron flux at ν_m[GHz]
$F_{\rm x}$ [Jy]: X-ray flux at ν_x[keV]
$\theta_{\rm d}$ [mas]: VLBI core size
$\nu_{\rm b}$ [Hz]: Synchrotron high frequency cutoff
α: Optically thin synchrotron spectral index
$f(\alpha) \simeq 0.08\alpha + 0.14$ (Ghisellini et al. 1993)

We calculated Doppler factors $\delta_{\rm IC}$ from the compilation of VLBI data by Ghisellini et al. (1993) and the ROSAT PSPC fluxes at 1 keV; α = 0.75 and $\nu_{\rm b}$ = 10^{14}Hz was assumed. The results are given in Table 3. The distribution of the objects in the $\alpha_{\rm rx} - \delta_{\rm IC}$ and $\alpha_{\rm x} - \delta_{\rm IC}$ planes in Fig. 8 show a strong correlation of $\delta_{\rm IC}$ with $\alpha_{\rm rx}$. As the subsample with available VLBI data contains predominantly RBLs, which show an anticorrelation of $\alpha_{\rm rx}$ and $\alpha_{\rm x}$, $\delta_{\rm IC}$ and $\alpha_{\rm x}$ are also anticorrelated. Looking at Eq. (1) two reasons may be responsible for the correlation of $\alpha_{\rm rx}$ and $\delta_{\rm IC}$:

1. The values of $\delta_{\rm IC}$ must be considered as lower limits, as direct synchrotron emission may contribute to or even dominate the X-ray flux and thus the inverse Compton flux $F_{\rm IC}$ is overestimated. In this case $\delta_{\rm IC}$ will be underestimated by the factor

$$\delta_{\rm true}/\delta_{\rm IC} = (F_{\rm x}/F_{\rm IC})^{-1/5.5}$$

Assuming that the diversity in

$$\alpha_{\rm rx} = (\log_{10}(F_{\rm 5GHz}) - \log_{10}(F_{\rm 1keV}))/7.68$$

is caused by a more or less energetic synchrotron component,

$$\delta_{\rm true}/\delta_{\rm IC} = 10^{1.40\cdot\alpha_{\rm rx}}$$

results. This function is indicated in Fig. 8 a) as solid line.

2. Both $\alpha_{\rm rx}$ and $\delta_{\rm IC}$ depend on the radio flux of the source. The total fluxes $F_{\rm 5GHz}$ determining $\alpha_{\rm rx}$ and the VLBI core fluxes F_m strongly correlate. Varying the core flux $F_{\rm m}$ and $F_{\rm 5GHz}$ by the same factor while leaving $F_{\rm x}$ constant results in

$$\delta_{\rm IC} \propto 10^{7.68\cdot\alpha_{\rm rx}}$$

as indicated by the dashed line in Fig. 8 a).

Figure 8 shows that the first possibility, overestimation of the Compton flux, cannot fully account for the measured correlation and viewing angle effects cannot be ruled out to cause the differences in $\delta_{\rm IC}$.

Ghisellini et al. (1993) noted that BL Lacs show a broader distribution of $\delta_{\rm IC}$ than flat spectrum radio quasars (FSRQs) with a tail towards low values of $\delta_{\rm IC}$. It is apparent from Fig. 8 that one group of objects has properties very similar to flat spectrum radio quasars: flat X-ray spectra, $\alpha_{\rm rx} \sim 0.9$, and $\delta_{\rm IC}$ = 1..10. The corresponding properties of FSRQs are: $\langle\alpha_{\rm x}\rangle$ = 0.59, $\langle\alpha_{\rm rx}\rangle$ = 0.88, (Brunner et al. 1994), $\delta_{\rm IC}$ = 1..10 (Ghisellini et al. 1993). The remaining RBL objects have steeper X-ray spectra, lower $\alpha_{\rm rx}$ and lower $\delta_{\rm IC}$.

7. EGRET detected objects

8 objects of the sample have been detected in high energy γ-rays (>100 MeV) by EGRET on the Compton Gamma Ray Observatory: AO 0235+16, PKS 0537-44, S5 0716+71, S4 0954+65, MARK 421, ON 231, PKS 2005-48 (4–5σ), and PKS 2155-30 (von Montigny et al. 1995, Vestrand et al. 1995). The EGRET objects are indicated by filled symbols in Figs. 2 and 8. All these objects except the low distance XBLs MARK 421 and

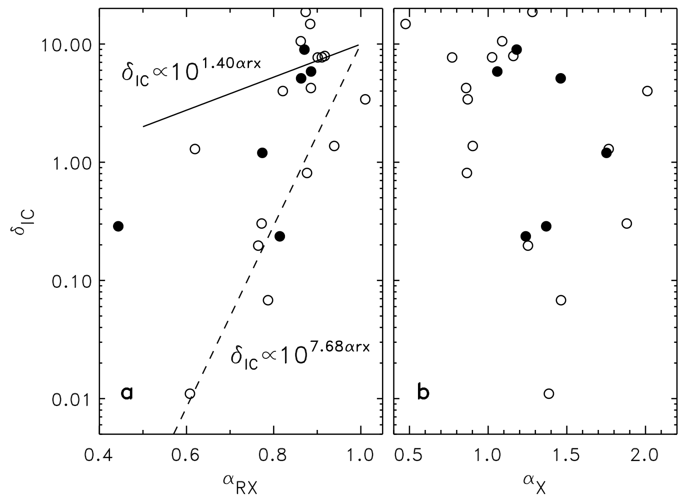

Fig. 8. a) Inverse Compton beaming factor δ_{IC} vs. α_{rx} . b) δ_{IC} vs. X-ray spectral index (filled circles: EGRET detected objects).

PKS 2155-304 have $\alpha_{rx} > 0.7$. As can be read from Fig. 2, the EGRET sources show the same $\alpha_{rx} - \alpha_x$ dependence as the remaining objects. Note that not only "FSRQ-like" BL Lac objects have been detected by EGRET, but also objects with steep X-ray spectra and moderate δ_{IC} .

8. Comparison with other ROSAT studies

During the refereeing process of this paper we learned that a number of ROSAT studies using different BL Lac samples are going to be published. In this section we will briefly discuss their results in comparison with ours.

Based on an analysis of 12 objects from the 1 Jy sample Comastri et al. (1995) show that the more radio bright objects ($\alpha_{rx} > 0.75$) in their radio selected sample on average have flatter X-ray spectra than the more X-ray bright ($\alpha_{rx} < 0.75$) ones. As their sample covers only the radio bright part of the α_{rx} distribution, this finding fits well to our overall picture of the spectrum of BL Lacs, where objects of intermediate α_{rx} do have the steepest X-ray spectra.

A detailed investigation of the ROSAT observations of the 1 Jy sample has been undertaken by Urry et al. (1996). The above authors both interprete steep X-ray spectra of BL Lacs as a sign for synchrotron emission, while flat X-ray spectra should be dominated by self-Compton emission. Perlman et al. (1996) performed a ROSAT investigation of the EMSS XBL sample and found a distribution of X-ray spectra similar to the 1 Jy sample.

By considering the whole sample of BL Lac objects we are able to verify the view, that BL Lacs except the extreme RBLs are dominated by synchrotron emission. We show that the extreme XBLs have flat X-ray spectra caused by synchrotron spectra with cutoff energies beyond the soft X-ray band. Our spectral simulations yield a good measure for the synchrotron cutoff energy and show that the range of cutoff energies is large.

Padovani&Giommi (1996b) have calculated X-ray spectral indices in a large sample of BL Lacs from hardness ratios provided by the ROSAT WGA catalogue (White et al. 1994) and with this method obtain a similar dependency of α_x on the radio to X-ray flux ratio as we do.

9. Discussion

We find that the broad distribution of spectral slopes in the soft X-ray spectra of BL Lacs is due to a strong dependence of α_x on the broad band spectral index α_{rx} . Objects with extreme values of α_{rx} exhibit flat X-ray spectra, whereas intermediate objects have steeper spectra. The symmetry of this dependence prevented the detection of significant differences between the mean X-ray spectra of XBLs and RBLs in previous investigations (Worrall & Wilkes 1990, Sambruna et al. 1994, Lamer et al. 1994).

By comparison with simulated PSPC spectra we showed that a two component model with a hard power law ($\alpha = 0.7$) component and a steepening soft component is appropriate to explain the observed spectra. The frequency where the components intersect each other is below the soft X-ray band for extreme RBLs and crosses the energy band of the ROSAT PSPC with declining α_{rx} . In the framework of the SSC models this means that Compton emission causes the flat X-ray spectra of extreme RBLs, whereas the likewise flat X-ray spectra of extreme XBLs are due to synchrotron emission. The steep X-ray spectra of objects with intermediate spectral energy distribution ($0.6 < \alpha_{rx} < 0.8$) represent the first direct evidence of the synchrotron high energy cutoff.

Padovani & Giommi (1995) explain the different spectral energy distributions of XBLs and RBLs by different energy cutoffs of the synchrotron spectra. They postulate the cutoff energy being intrinsic properties of the sources without discussing the physics of the emission processes. This scenario also is the most straightforward explanation for our findings, including the correlation of α_{rx} and α_x for the XBL subsample. The wide range in synchrotron cutoff energies, and consequently the cutoff in the energy spectrum of the relativistic electrons, has to be explained. The SSC cooling of the jet electrons may be more efficient in the more powerful jets of FSRQs and RBLs than in the jets of XBLs. Ghisellini & Maraschi (1994) proposed a more rapid cooling of jet electrons in FSRQs by external UV photons compared to jets of BL Lac objects. It is conceivable that RBLs are intermediate objects between XBLs and FSRQs regarding the ambient photon density.

The more physically motivated beaming models, such as the "accelerating jet" model (Ghisellini & Maraschi 1989) and the "wide jet" model (Celotti et al. 1993) do not as naturally satisfy our data. The crossover frequencies of soft and hard components in the spectra calculated by Ghisellini and Maraschi (1989) do not span a sufficient range and do not move across the soft X-ray range when tilting the viewing angle, as required by the new data. Nevertheless, further tuning of the free parameters may provide spectra which are in accordance with the measurements. The ROSAT spectra therefore are suitable to constrain the beaming models.

Acknowledgements. This work was supported by DARA under grant 50 OR 90099 and has made use of the NASA/IPAC Extragalactic Database (NED) which is operated by the Jet Propulsion Laboratory, Caltech, under contract with the National Aeronautics and Space Administration.

References

Brunner, H., Lamer, G., Worrall, D.M., and Staubert, R. 1994, A&A, 287, 436
Celotti, A., Maraschi, L., Ghisellini, G., Caccianiga, A., and T. Maccacaro, 1993, ApJ, 416, 118
Ciliegi, P., Bassani, L., and Caroli, E. 1995, ApJ, 439, 80
Comastri, A., Molendi, S., and Ghisellini, G. 1995, MNRAS, in press
Eckart, A., Witzel, A., Biermann, P.L., et al. A&A, 168, 17
Elvis, M., Lockman, F.J., and Wilkes, B.J, 1989, AJ, 97, 777
Ghisellini, G., Maraschi, L., and Treves, A., 1986, A&A, 146, 204
Ghisellini, G. and Maraschi, L., 1989, ApJ, 340, 181
Ghisellini, G., Padovani, P., Celotti, A., and Maraschi, L., 1993, ApJ, 407, 65
Ghisellini, G., and Maraschi, L., 1994, in *The second Compton Symposium*, AIP Proceedings 304, eds. C.E. Fichtel, N. Gehrels, and J.P. Norris, 616
Giommi, P., Barr, P., Garilli, B., Maccagni, D., and Pollock, A.M.T., 1990, ApJ 356, 432
Kock, A., Meisenheimer, K., Brinkmann, W., Neumann, M. and Siebert, J. 1996, A&A, in press
Königl, A., 1981, ApJ, 243, 700
Lamer, G., Brunner, H., Staubert, R., 1994, in *Multi-Wavelength Continuum Emission of AGN*, eds. T.J.-L. Courvoisier & A. Blecha (Dordrecht: Kluwer), p. 377
Maraschi, L. and Rovetti, F., 1994, ApJ, 436, 79
Marscher, A.P., 1987, in *Superluminal Radio Sources*, eds. A. Zensus & T.J. Pearson (Cambridge Univ. Press), 280
Morris, S.L., Stocke, J.T., Gioia, I.M., et al. 1991, ApJ, 380, 49
Morrison, R., and McCammon, D., 1983, ApJ, 270, 119
Nass, P., Bade, N., Kollgaard, R.I. 1996, A&A, in press
Padovani, P. and Urry, C.M., 1990, ApJ, 356, 75
Padovani, P. and Giommi, P., 1995, ApJ, 444, 567
Padovani, P. and Giommi, P., 1996a, MNRAS, in press
Padovani, P. and Giommi, P., 1996b, MNRAS, in press
Perlman, E., Stocke, J. T., Wang, Q. D., et al. 1996, ApJ, in press
Sambruna, R.M., Barr, P., Giommi, P., et al. 1994, ApJ, 434, 468
Stark, A.A., Gammie, C.F., Wilson, R.W. et al., 1992, ApJS, 79, 77
Stickel, M., Padovani, P., Urry, C.M., Fried, J.W., and Kühr, H., 1991, ApJ, 374, 431
Stickel, M., Meisenheimer, K., and Kühr, H., 1994, A&AS, 105, 211
Urry, C. M., Sambruna, R. M., Worrall, D. M., et al. 1996, ApJ, submitted
Véron-Cetty, M.P., and Véron, P., 1993, ESO Scientific Report, 13
Vestrand, W.T., Stacy, J.G., and Sreekumar, P. 1995, IAU Circ. 6169
Von Montigny, C., Bertsch, D.L., Chiang, J., et al. 1995, ApJ, 440, 525
White, N. E., Giommi, P., and Angelini, L., 1994, IAU Circ. 6100
Worrall, D.M., 1989, Proc. 23rd ESLAB Symp., ESP SP-296, 719
Worrall, D.M., and Wilkes, B.J, 1990, ApJ, 360, 396
Zimmermann, H.U., Belloni, T., Izzo, C., Kahabka, P., Schwentker, O., 1993, EXSAS User's Guide, MPE Report 244

This article was processed by the author using Springer-Verlag LaTeX A&A style file *L-AA* version 3.